RSC Advances

PAPER

View Article Online
View Journal | View Issue

Cite this: *RSC Adv.*, 2025, **15**, 29743

Water confinement in carbon nanocones: molecular dynamics study

Kichan Chun,†[a] Yeeun Lee,†[b] Jian Jeong,†[bc] Gunn Kim *[a] and Soonmin Jang *[b]

Received 11th July 2025
Accepted 11th August 2025

DOI: 10.1039/d5ra04968g

rsc.li/rsc-advances

The confinement of water molecules within nanostructures is a subject of intense research. Unlike carbon nanotubes (CNTs), carbon nanocones (CNCs) possess a conically expanding cross section, providing significantly different confinement environments within the CNT. In this study, we employed classical molecular dynamics simulations to investigate how the structural and dynamic properties change along the CNC axis, from the base to the tip, and from the water–carbon interface to the interior of CNCs, under varying tip angles. The simulations reveal a high sensitivity of the nanoconfined water structure to the tip angle. Notably, local confinement within CNCs influences water structure up to 15 Å away. The water density exhibits strong modulation in a layered fashion near the CNC interface, depending on the tip angle, indicating complex geometric dependencies. These findings offer new insights into water–CNC interactions and nanoscale confinement, with implications for understanding the unique behavior of water and its potential applications in nanostructured systems.

1 Introduction

In recent decades, extensive research has shown that water molecules confined within nanostructures, sometimes in combination with biomolecules, exhibit unique structural and dynamic properties that differ significantly from those of bulk water.[1–5] This confinement effect has led to a wide range of applications in fields such as gas separation,[6–8] water desalination,[9–11] DNA detection,[12] and drug delivery.[13] Both experimental and theoretical research have examined the physical and chemical properties of various nanosized systems, particularly focusing on the structure and dynamics of confined water under diverse geometric and material constraints.[1,14] Water confined within nanometre-scale spaces displays fundamentally different density and phase transition properties compared to bulk water,[15] including melting and freezing.[16] Such confinement not only permits the coexistence of distinct water phases within individual carbon nanotubes (CNTs)[17,18] and the interlayer space of graphene[19] but also promotes the formation of low-dimensional ice, exhibiting diverse structural motifs.[20,21] Barati Farimani *et al.*[17] observed continuous phase transitions of water molecules along the direction of the CNT radius, including a one-molecule-layer, so-called "ice-like structure"[18,22] characterized by low entropy, which can occur under high pressure and density within CNTs of radii ranging from 1 to 4 nm. Recently, Fang *et al.*[23] investigated water molecules at the 1-D/2-D heterojunction by arranging CNTs of various sizes between two graphene sheets, discovering structural rearrangements in water, particularly in the case of small-diameter CNTs.

In addition to the extensive research on carbon nanotubes and graphene, carbon nanocones (CNCs), a unique form of bent carbon,[24] have also been studied for their unique properties, including structural,[25,26] electronic,[27,28] mechanical,[29,30] and thermal properties.[31] This has stimulated investigations into their potential applications, including desalination,[32,33] sensing,[34,35] and thermal rectification,[36] in both pristine and doped cases. The development of various synthesis techniques, such as cascade annulation[37] and pyrolysis for scalable production, has further stimulated research interest in CNCs.[32,38,39]

Although the behaviour of confined water in carbon-based nanomaterials, particularly CNTs and graphene, has been extensively studied, revealing distinct water phases influenced by the geometry and nature of the confinement,[40,41] similar studies on CNCs remain scarce. The unique geometry of CNCs produces a continuous confinement gradient within a single structure. As the cross-section widens from tip to base, water molecules experience strong confinement near the tip that gradually transitions to near-bulk conditions at the base. Consequently, CNCs provide a compelling platform to study the effects of continuously evolving nanoconfinement on fluids such as water within a single carbon-based system. In this study, we aim to reveal the detailed structure and dynamics of

[a]*Department of Physics and Astronomy, Sejong University, Seoul 05006, South Korea. E-mail: gunnkim@sejong.ac.kr*

[b]*Department of Chemistry, Sejong University, Seoul 05006, South Korea. E-mail: sjang@sejong.edu*

[c]*inCerebro, Seoul 06234, South Korea*

† These authors contributed equally.

water molecules in CNCs, with a focus on their density, hydrogen bonding, dipole moment orientation, and the orientational diffusion. Since the degree of confinement is governed by both the distance from the tip and the tip angle, we used molecular dynamics simulations to investigate how the structural and dynamic properties of water molecules within CNCs vary as a function of the tip angle.

2 Methods

The tip of CNCs is characterized by the presence of pentagonal carbon rings, the number of which is determined by the tip angle.[26] For this study, we selected three CNC models with varying tip angles: 86.6° (P2), 60.0° (P3), and 38.9° (P4). These models are distinguished by the number of pentagons at the cone vertex, specifically two for P2, three for P3, and four for P4. Although CNCs with a 112.9° tip angle have been reported,[38] they were excluded from the present investigation. The three types of CNC models we studied are shown in Fig. 1a and b. Each CNC model had a similar height of approximately 40 Å. To examine the effect of height (*i.e.*, the distance from the tip to the CNC base) on water structure and dynamics at a fixed tip angle, we also included two additional P3 models: P3-s (25 Å) and P3-l (55 Å). The CNC structures were initially constructed using Nanotube Modeler[42] and modified with GaussView6.[43] In the simulations, each CNC was placed at the centre of a dodecahedral simulation box, maintaining a minimum distance of 20 Å from the box boundaries to minimize interaction artifacts. The system was then solvated with water molecules, and periodic boundary conditions were applied in all three dimensions. Detailed information about the simulation box is given in Table S1.

For modeling the CNCs, we used the OPLS-AA force field,[45] and the Simple Point Charge/Extended (SPC/E) water model[46] was employed to represent water. Additionally, to assess the water model dependency, we also used another water model, the TIP4P-Ew water.[47] It is worth noting that the SPC/E model has been widely used in previous studies of confinement effects,[48–52] including investigations of phase coexistence and density variation in CNT-confined water.[17] While the SPC/E model reproduces key properties of liquid water, such as density, structure, and diffusion coefficients, it has limitations in describing the dielectric constant. In contrast, the TIP4P-Ew model better accounts for the dipole moment and many thermodynamic quantities due to electrostatic corrections, though it also struggles to capture the flexible nature of water, similar to SPC/E. The choice of water model should be guided by the specific properties of interest, simulation conditions, and computational constraints. Both SPC/E and TIP4P-Ew are widely used and offer reasonable accuracy for many liquid water properties; however, no model is universally perfect, and simulation results should be validated against experimental data whenever possible. After solvation, energy minimization was performed using the steepest descent method, followed by 200 ps of constant volume constant temperature (NVT) simulation. This was followed by 200 ps of constant pressure constant temperature (NPT) simulation, and then a 5 ns NPT simulation as the production run. The LINCS algorithm[53] was employed to maintain the carbon–carbon bond distance of the CNCs under an all-bonds constraint, as the CNCs are highly flexible under water solvation conditions.[54] The temperature and pressure were set to 300 K and 1 atm, respectively. Temperature was controlled using the velocity rescaling method[55] with a coupling constant of 0.1 ps, while pressure was maintained using the Berendsen pressure coupling method[56] with a coupling constant of 16 ps. Throughout the study, position restraint with a constant of 1000 (kJ mol^{-1} nm^{-2}) were imposed on the CNC carbon atoms. The leap-frog integrator method was used for time propagation with an integration time step of 1 fs, and positions were saved every 100 steps. For the final analysis, we used the last 2 ns of the NPT production simulation trajectories, which contained 20 000 frames.

To compute water density and hydrogen bonding within CNCs, we defined two coordinates for locating each water molecule: the axial distance from the tip (z), and the radial distance from the central axis toward the nearest carbon wall (r), as illustrated in Fig. 1(c). The central axis was defined as the line connecting the cone's vertex to the centre of mass of the carbon atoms at the base. The cone tip angle θ is related to z and r as follows

$$\sin\left(\frac{\theta}{2}\right) = \frac{r}{z} \tag{1}$$

The oxygen atom's position was used to represent the location of each water molecule. We estimated the number density of water molecules within each spatial bin by averaging over 20 000 frames. Given the confinement of water molecules in the CNC, we used a bin size of 1.0 Å both along the z and r coordinates.

Hydrogen bonds (HBs) were defined based on geometric criteria: the distance between the oxygen atoms of two different water molecules must be less than 3.5 Å, and the angle O···O–H must be less than 30°,[57–60] where "···" denotes a hydrogen bond and "–" represents a covalent bond. We also estimated the intermittent hydrogen bond lifetime from the hydrogen bond correlation time $C_{HB}(t)$ as follows[17,61]

$$C_{HB}(t) = \frac{\langle h(t) \times h(0) \rangle}{\langle h(0)^2 \rangle}, \tag{2}$$

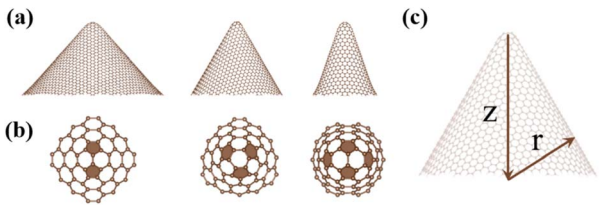

Fig. 1 Structures of the three CNCs studied. (a) Side views. (b) Top views highlighting pentagonal rings near the tip (shaded for clarity). (c) Coordinate system for specifying water molecule positions. All illustrations were generated using VESTA.[44]

where $h(t)$ equals 1 if the hydrogen bond exists at both time 0 and time t, and 0 otherwise. The hydrogen bond lifetime τ is defined as $\tau = \int_0^\infty C_{HB}(t)dt$. To analyse water molecule rotational dynamics, additional NPT simulations of 50 ps was conducted starting from the last structure of 5 ns production run. For this purpose, we used 0.5 fs time step and last 30 ps of trajectories, *i.e.*, 60 000 frames, are used for estimation of rotational diffusion constant (D_r).[17,62–64] This quantity can be estimated by tracking the time-dependent polarization vector, $p_i(t)$, for the i-th water molecule. For each molecule, this vector was defined as the normalized vector pointing from the molecule's centre of mass to the midpoint between its two hydrogen atoms. Over time interval $[t, t + \delta t]$, the vector $p_i(t)$ rotates by an angle $\delta\theta$, given by $\delta\theta = \cos^{-1}[p_i(t) \times p_i(t + \delta t)]$. A new vector $\delta\vec{\varphi}_i(t)$ is then defined such that its magnitude equals $\delta\theta$ and its direction is determined by the cross product $p_i(t) \times p_i(t + \delta t)$ expressed as

$$\delta\varphi_i(t) = \delta\theta \times \frac{p_i(t) \times p_i(t + \delta t)}{\|p_i(t) \times p_i(t + \delta t)\|}. \quad (3)$$

Subsequently, the rotational motion of the molecule is represented by the vector $\vec{\varphi}_i(t) = \int_0^t \delta\vec{\varphi}_i(t')dt'$. Thus, the vector $\vec{\varphi}_i(t)$ defines the trajectory within φ-space, which characterizes the rotational motion of water molecule i. The schematic diagram is shown in Fig. S6. The trajectory is then used to calculate the rotational mean-square angle displacement (MASD), expressed as:

$$\langle\varphi^2(t)\rangle = \frac{1}{N}\sum_i \left|\vec{\varphi}_i(t) - \vec{\varphi}_i(0)\right|^2 \quad (4)$$

The rotational diffusion coefficient is given by:

$$D_r = \lim_{t\to\infty}\frac{1}{4t}\langle\varphi^2(t)\rangle \quad (5)$$

3 Results and discussion

3.1 Analysis of water density in carbon nanocones

The average densities of SPC/E water in the P2, P3, and P4 CNCs were found to be 0.96, 1.00, and 0.84 g cm^{-3}, respectively. The cross-sectional snapshots of the CNCs are presented in Fig. S1. To investigate how confinement and surface properties affect the water structure, we calculated the position-dependent water densities within each CNC, as shown in Fig. S2, plotted as a function of radial distance r at various z-coordinates. Starting from the carbon wall, large r, a rapid increase in density is observed, forming a pronounced peak with maximum density, followed by moderate fluctuations that eventually stabilize to the bulk water density as the radial distance is decreased in general. Prior studies of water confined within simple carbon-based nanostructures have reported similar behaviours, attributing them to interfacial effects between the water and the hydrophobic carbon surface.[65,66] Clearly, water density and structure are highly sensitive to the local environment, particularly the confining geometry. For example, Barati Farimani *et al.*[17] showed that the detailed interfacial water density in CNT varies with the tube radius and exhibits a complex, nontrivial pattern. Han *et al.*[67] calculated the density–temperature (ρ–T) phase diagram of water confined between hydrophobic plates using molecular dynamics simulations. High-density water regions have been reported to exhibit rhombic structures,[68,69] such as in Barati *et al.*'s (10, 10) CNT study at 300 K and Han *et al.*'s work across 230–310 K. The formation of the ice structure, ice VII phase, was also confirmed in an experiment using surface-enhanced Raman spectroscopy by Shin *et al.*, for water molecules confined within narrow inter-particle gaps.[70,71] The overall densities with SPC/E water are visualized as heatmaps in Fig. 2. In this study, water density was classified into three regions: low (ρ < 0.65 g cm^{-3}), medium (0.65 ≤ ρ ≤ 2.0 g cm^{-3}), and high (ρ > 2.0 g cm^{-3}).

In Fig. 3, we re-plot Fig. 2 based on these three densities with different colours (red: low, blue: medium, and yellow: high). The formation of the high-density water layer near the carbon wall is thought to arise from reduced entropy and elevated pressure, driven by van der Waals interactions between water molecules and the hydrophobic carbon surface.[67] We note that the thickness of this high-density region is approximately a single layer of water molecules. In all CNCs here, the high-water density is manifested near the tip region and presumably attributed to the pronounced confinement in this region. Near the tip region, water molecules experience increased dewetting[72] due to stronger hydrophobic interactions with the carbon atoms, which in turn further enhances the water density fluctuations observed at the surface. A clear trend in both Fig. 2 and 3 is that decreasing the tip angle, thus increasing confinement, results in significantly elevated water density extending along the carbon wall. For example, the density of water molecules near the carbon atom in P4 is much higher than in P3 and P2 at the same radial distance of $r = 10$ Å. Given that high water density near the carbon surface is due to short-range van der Waals interaction this is a somewhat unexpected. In these regions, the axial distances from the tip are 10.6 Å for P2, 17.3 Å for P3, and 28.3 Å for P4. Therefore, this unexpectedly high-density near the carbon atom in P4 at $r = 10$ Å cannot be

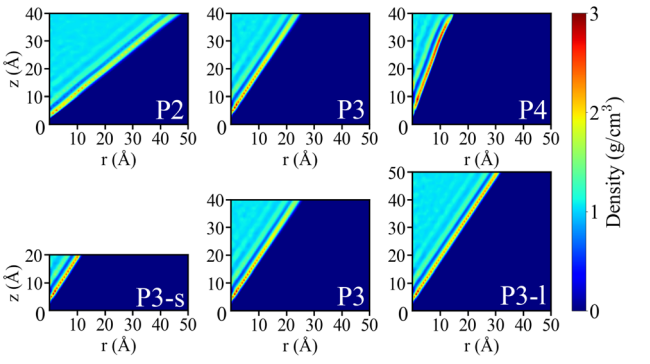

Fig. 2 Heat maps depicting the densities of SPC/E water within CNCs of varying tip angles, plotted as a function of radial distance r and vertex height z.

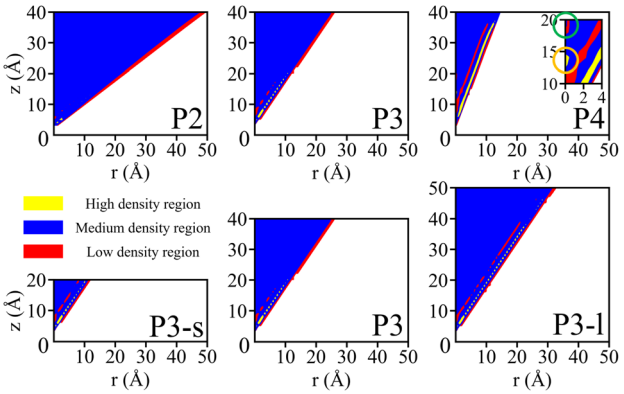

Fig. 3 Phase distributions of SPC/E water molecules in each CNC plotted as a function of vertex height z and central distance r. The phases are determined based on the densities shown in Fig. 2.

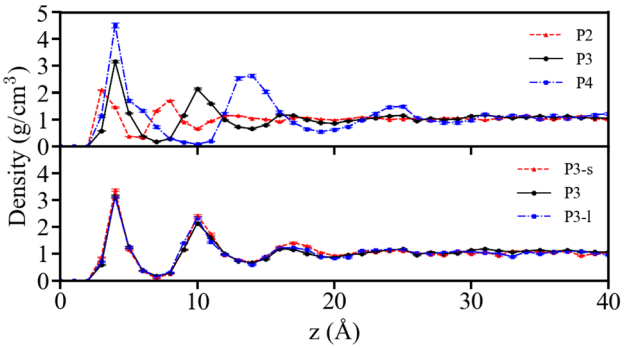

Fig. 4 Water densities plotted as a function of vertex height z near $r = 0$. For practical purpose, we have used waters within $r = 0.8$ Å.

solely attributed to proximity to the tip. Instead, as the tip angle decreases, the gradually narrowing geometry enhances spatial constraints on water molecules near the CNC surface.

The more gradual confinement changes in P4, compared to P2 and P3, may preserve a well-ordered hydrogen-bond network extending from the tip region. These results of distinct variations in water structure among CNCs with different tip angles indicate that water structure due to local confinement can influence the arrangement of water in distant regions, even beyond 10 Å.[73] The observation that water density at the same r remains unchanged across P3-s, P3, and P3-l, despite differences in height, further supports this interpretation. Meanwhile, the high-density region is further extended towards the base in the P3-l CNC, suggesting that the water structure at a given z and r is different depending on the total height of the CNC. Specifically, at $r = 15$ Å, the density near the interface of P3-l is more pronounced than its counterpart in P3. This suggests that the density fluctuation, including the high-density region observed around $r = 15$ Å in P3-l, is driven by local confinement effects. In contrast, P3 does not show this density fluctuation at the same r, likely due to direct exposure to bulk water outside the cone, which dominates the local water structure. In other words, the extended confinement in P3-l, due to its greater height, may allow for local density separation at $r = 15$ Å, which is suppressed in P3 by the nearby bulk water environment. Similarly, in P3-s, the persistence of confinement originating from the tip may dominate over bulk water effects near the base, leading to extended density fluctuation.

Interestingly, noticeable density separation was observed not only in strongly confined regions near the CNC tip and carbon wall but also in weakly confined or unconfined regions distal from these boundaries, as shown in Fig. 3. In Fig. 3, the density at $0 \leq r \leq 4$ and $10 \leq z \leq 20$ is magnified as inset in P4 and distinct density separation at $r = 0$ can be observed along the z axis as indicated with orange (high density region) and green (low density region) circles $z = 14$ Å and $z = 18$ Å, respectively. This is more clearly illustrated in Fig. 4, which plots the water density along the tip-to-base direction (the z axis) corresponding to central axis (near $r = 0$). Overall, as the tip angle decreases, the deviation of water density from bulk water becomes more pronounced along the z-axis. In particular, P4 exhibits dramatic density variations, with two high-density peaks at 4.8 g cm^{-3} ($z = 4$ Å) and 2.8 g cm^{-3} ($z = 14$ Å). Between these peaks, the density drops sharply, approaching zero, where volume available to water is most restricted due to enhanced dewetting as mentioned earlier. The first peak observed (blue line) near $z = 5$ Å is attributed to this high degree of spatial confinement that enhances structuring and layering of water, leading to sharp density features even close to the axis. The first peak (blue line for P4) near $z = 5$ Å is attributed to strong confinement near the CNC tip. However, the appearance of the second peak around $z = 14$ Å was unexpected, as it lies relatively far from the tip and outside the most confined region. Likely, this severe, continuous density variation is mainly induced by the intense confinement near the tip, extending up to approximately $z = 15$ Å and another local density maximum near 25 Å. Similar but less pronounced trends are observed in P2 and P3, likely due to weaker confinement at their tips. These findings suggest that the tip's confinement effect can propagate over distances exceeding 10 Å, depending on the geometry of the surrounding carbon atoms. These central density fluctuations are influenced not only by tip-induced confinement but also by the short radial distance to the carbon wall in P4. Long-range structural influence exceeding 10 Å has also been reported in other studies.[24] For P3 variants of different lengths, density profiles along $r = 0$ indicate that the peak shapes are preserved.

3.2 Analysis of HB bond, dipole moment orientation, and rotational diffusion constant

The water hydrogen bond (HB) is a key indicator of the water structure and dynamic behaviour. We show a heatmap in Fig. 5 depicting the number of HBs in each CNC as a function of the distance from the radial distance (r) and vertex height (z), consistent with the density plot shown in Fig. 2. Across all CNCs, the average number of HBs is approximately 3.7 except near the carbon wall where it decreases. We overlapped the calculated number of HB with water density in each CNC as a function of the central axis (r) at the specific vertex height (z) in Fig. S2. The number of HBs remains constant inside the CNC but gradually decreases toward the carbon wall as the water

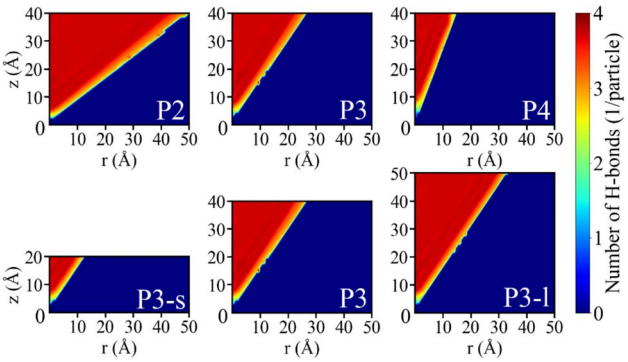

Fig. 5 Heat map of the number of hydrogen bonds in CNCs as a function of r and z.

molecules have fewer neighbouring water molecules to form hydrogen bonds near the carbon wall.[19,66] The results obtained using the TIP4P-Ew model (Fig. S3–S5) show trends similar to those of the SPC/E model, though with slightly higher overall water density and hydrogen bond counts. Consequently, all subsequent analyses are based on the SPC/E water model.

To gain deeper insights into the density-dependent structural and dynamic properties in the P4 CNC, we analysed the intermittent HB lifetime correlation function and the distribution of water molecule dipole moment orientations in three different density regions near the carbon wall. Hereafter, the high-, medium-, and low-density regions refer to the yellow, blue, and red zones, respectively, as shown in the P4 plot of Fig. 3. Fig. 6(a) displays the time dependent hydrogen bond correlation function and the estimated HB life time indicates high density region near the carbon wall has the longest HB lifetime (6.53 ps), followed by the middle density region (4.52 ps) and the low-density region (1.36 ps). The reduced number of hydrogen bonds per molecule in the high-density region (Fig. S1) likely results from the limited availability of neighbouring water molecules beyond the carbon wall. The Fig. 6(b) illustrates the distribution of dipole moment orientation angles. This angle is defined as the angle difference between the dipole moment of water and the normal vector to the carbon wall surface toward inside of CNT. The high-density, medium-density, and low-density in the Fig. 6(a) and (b) regions are referring to the first yellow layer from the carbon surface, the blue layers next to it, and the red layers inside the CNC in Fig. 3 with P4, respectively. The figure reveals there is structural ordering, especially in high density layer, within these three different layers of water molecules near the CNC surface unlike water molecules inside of CNC (represented as bulk). The orientation angle around 100–110° indicate a majority of water molecules maintain one hydrogen atom directed towards the wall. It has been reported from both simulation and experimental studies that water molecules near hydrophobic surfaces, with some curvature dependency, often exhibit preferential orientations with O–H bond toward surface, even in the absence of direct hydrogen bonding with the surface[40,74,75] to minimize the broken HBs. Although the hydrophobic wall cannot accept hydrogen bonds, this orientation allows the oxygen atoms of interfacial water molecules to remain accessible to form hydrogen bonds with adjacent water molecules in the bulk or second layer. In contrast, water molecules in the medium and low-density regions exhibit weaker orientational ordering, although the medium region shows slightly more structure than bulk water. The prolonged HB lifetime in the high-density region likely results from enhanced water–water interactions and significant dipole moment alignment.

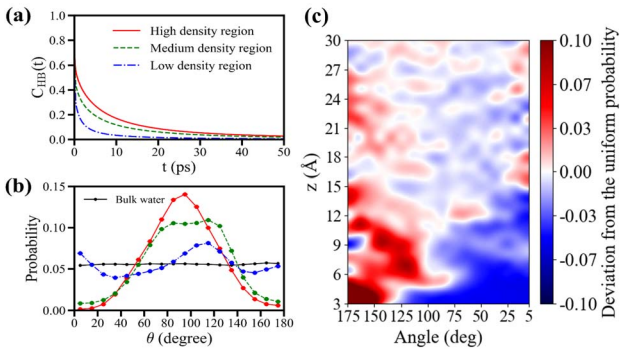

Fig. 6 (a) The intermittent hydrogen bond lifetime correlation function for the three distinct water phases (layers) in P4. (b) The dipole moment orientation distribution of three different water phases (layers) of P4. For each water a vector is defined by connecting the oxygen atom of a water molecule and the nearest carbon atom to it. (c) The dipole moment angle distribution near the centre of radial distance along the z-axis in the P4 CNC. It is represented as the deviation of probability from the average probability of bulk water orientation. The red area means a high dipole moment ordering region compare to bulk water, and the blue area means regions with less orientational propensity compare to bulk water. The water molecules within the radius of 0.8 Å were selected for this plot.

As noted earlier, strong density variation is observed along the z-axis near the central radial region. To characterize this region, we analysed the dipole orientation distribution along the z-axis, shown in Fig. 6(c). Near the tip, water molecules exhibit strong orientation, which gradually diminishes with increasing z. Notably, the low-density region near $z = 9$ Å and the high-density region near $z = 14$ Å exhibit distinct orientation angles of approximately 140° and 175°, respectively.

As an additional dynamic measure, we computed the time-dependent rotational mean square angular displacement (MSAD) for the first three density layers in P4, and presented in Fig. 7. The estimated diffusion coefficient (D_r) of high, medium, and low-density regions from these plots is 0.097, 0.096, and 0.171 (rad^2 ps^{-1}), respectively, which can be compared with the bulk SPC/E water D_r of 0.184 (rad^2 ps^{-1}). Due to the narrow spatial bins defining each density region, long-term tracking of water molecules was limited in our simulations. To obtain reliable slopes, we fitted the MSAD data linearly beyond 0.8 ps, excluding initial transients; the fits are shown as dashed lines. All three D_r values are lower than that of bulk water, with the low-density region showing the highest rotational mobility among the confined layers. The high- and medium-density regions exhibit nearly identical rotational dynamics.

Overall, water structure and dynamics within the CNCs vary significantly depending on the position specific confinement.

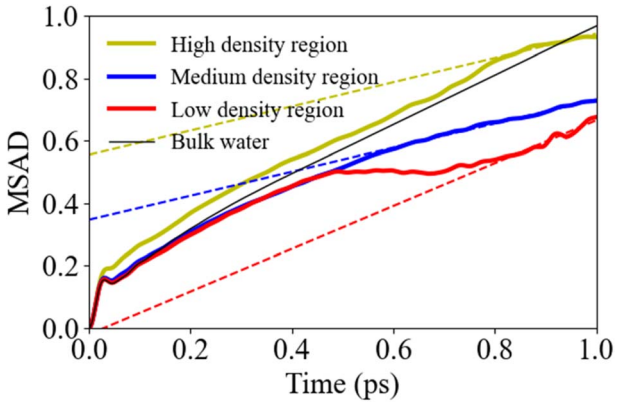

Fig. 7 The rotational mean square angle deviation (MSAD) of three different density regions as a function of time for P4.

We examined structural and dynamic features such as hydrogen bonding, dipole orientation, HB lifetime, and rotational diffusion coefficients. Our density-based analysis shows that high-density regions exhibit more rigid and ordered structures, while lower-density regions display reduced ordering and greater molecular mobility. A key finding is that local water structuring is affected not only by immediate confinement but also by global geometric features located farther away.

4 Conclusions

The behaviour of water molecules within nanoscale environments, especially near the interface with the confining atoms, is markedly altered by the dimensions and geometry of the confining space. In this study, we employed molecular dynamics simulations to investigate the structure and dynamics of water molecules confined within CNCs, a unique class of nanostructures that offer a continuous spectrum of confinement degrees within a single system. Our findings reveal a significant spatial heterogeneity in water density within the CNCs, varying as a function of both the radial distance from the central axis and the axial height. Specifically, the highest water density was consistently observed in the vicinity of the cone wall, exhibiting a gradual decrease with increasing distance towards the base. The observed confinement effects show quantitative difference within across different water models (SPC/E and TIP4P-Ew) here, as observed in previous studies,[76] but the general trends remains the same with only minor quantitative differences.

The current findings underscore the profound influence of the CNC geometry on the structure of the confined water, revealing notable dependencies on both the apex angle and the axial height of the CNC. The nanoconfinement imposed by the CNC significantly perturbs the local water structure, leading to substantial changes in the water density within the system. In particular, the high sensitivity of the confined water structure to the tip angle highlights the critical importance of precise geometric control in nanoscale water systems using CNCs. Our simulations also reveal a notable long-range effect, in which locally confined water molecules influence water structuring as far as 15 Å beyond the confinement region. This remarkable observation suggests that, depending on the intricate details of the confinement geometry, local confinement effects can propagate into regions where water would otherwise exhibit bulk behaviour. In essence, nanoscale confinement is not purely local; instead, water structure arises from a collective phenomenon where interactions from distant regions induce structural rearrangements in nearby molecules. These findings offer key insights into nanoconfinement physics and hold potential for designing advanced water filtration systems and improving predictive models of water behaviour in nanoscale environments. The demonstrated sensitivity of water structure to CNC geometry, coupled with the long-range effects of local confinement, provides promising avenues for the controlled manipulation of water behaviour in nanoscale systems.

In real-world systems, particularly those with biologically or chemically heterogeneous environments, nanoconfinement is rarely idealized. Instead, it often involves irregular geometries, surface roughness, and compositional inhomogeneities. For example, Wohlfromm and Vogel employed spatially resolved molecular dynamics simulations to show that confinement parameters (such as size and rigidity) strongly modulate the dynamic coupling between proteins and their hydration shells.[4] Similarly, studies of proteins inside carbon nanotubes, serving as model bio–nano interfaces, have revealed multiple adsorption substates along the tube interior, with water mobility decoupling according to the protein's adsorption state.[5] Moreover, investigations of water confined between chemically inhomogeneous sheets and/or pores demonstrate that surface chemistry, not just geometry, can dramatically alter hydration dynamics and induce strong spatial heterogeneity in water behaviour.[77,78] These features can dramatically influence water structure and dynamics, often in ways that differ from idealized systems such as the smooth, symmetric CNCs studied in this work.

The current work primarily focused on monitoring the structural aspects of water molecules inside CNCs, along with a dynamic property, the rotational diffusion coefficient. Future studies could explore additional structural, dynamic, and thermodynamic properties, such as viscosity, structural factors, and entropy.[17,79,80] Investigating these additional aspects would provide a more comprehensive understanding of water behaviour in nanoscale confinement.[81–83] Finally, we note that classical water models have inherent limitations, particularly concerning the non-transferable nature of water–carbon interactions at the interface, as shown in prior works.[84,85] Thus, future work could benefit from using more realistic models, such as those using machine learning-based force fields[86–88] or even *ab initio* molecular dynamics simulations[89–92] to overcome these limitations. By elucidating the intricate interplay between water and CNCs, this study advances our understanding of nanoscale confinement phenomena. It also sheds light on the unique behaviour of confined water, paving the way for future applications across a range of nanotechnology-related fields.

Author contributions

SJ and GK conceptualized and designed the study. KC, YL, and JJ conducted model setup, simulations, and data analysis. All authors contributed to data interpretation and participated in writing and editing the manuscript.

Conflicts of interest

There are no conflicts to declare.

Data availability

The carbon nanocone structure was built with Nanotube Modeler which can be downloaded from **http://www.jcrystal.com/products/wincnt/**. The molecular dynamics study was performed using GROMACS version 2021 which can be downloaded from **https://manual.gromacs.org/2021/download.html**. The in-house scripts for plotting were developed using Python3, and it is freely available at **https://www.python.org/download**.

Supplementary information contains detailed simulation box information as well as local density and hydrogen bond information as a function of radial distance. Also, results of TIP4P-ew water model are included. See DOI: **https://doi.org/10.1039/d5ra04968g**.

Acknowledgements

S. J. acknowledges financial support (Grant No. 2017M3D9A1073784) from the National Research Foundation of Korea (NRF). G. K. acknowledge the Basic Science Research Program's financial support (Grant No. NRF-2016R1A2B2016120 and NRF-2020R1A6A1A03043435) through NRF funded by the Government of Korea.

Notes and references

1 M.-C. Bellissent-Funel, Status of experiments probing the dynamics of water in confinement, *Eur. Phys. J. E*, 2003, **12**, 83–92.
2 R. Bergman and J. Swenson, Dynamics of supercooled water in confined geometry, *Nature*, 2000, **403**(6767), 283–286.
3 L. Bocquet, Nanofluidics coming of age, *Nat. Mater.*, 2020, **19**(3), 254–256.
4 T. Wohlfromm and M. Vogel, On the coupling of protein and water dynamics in confinement: Spatially resolved molecular dynamics simulation studies, *J. Chem. Phys.*, 2019, **150**, 245101.
5 P. Roy and N. Sengupta, Hydration of a small protein under carbon nanotube confinement: Adsorbed substates induce selective separation of the dynamical response, *J. Chem. Phys.*, 2021, **154**, 204702.
6 B. J. Hinds, N. Chopra, T. Rabtell, R. Andrews, V. Galvalas and L. G. Bachas, Aligned multiwalled carbon nanotube membranes, *Science*, 2004, **303**(5654), 62–65.
7 S. Kim, J. R. Jinschek, H. Chen, D. Sholl and E. Marand, Scalable fabrication of carbon nanotube/polymer nanocomposite membranes for high flux gas transport, *Nano Lett.*, 2007, **7**(9), 2806–2811.
8 W. Jeon, J. Yun, F. A. Khan and S. Baik, Enhanced water vapor separation by temperature-controlled aligned-multiwalled carbon nanotube membranes, *Nanoscale*, 2015, **7**(34), 14316–14323.
9 S. Kar, R. Bindal and P. Tewari, Carbon nanotube membranes for desalination and water purification: Challenges and opportunities, *Nano Today*, 2012, **7**(5), 385–389.
10 R. Das, M. E. Ali, S. B. E. Abd Hamid, S. A. Ramakrishna and Z. Z. Chowdhury, Carbon nanotube membranes for water purification: A bright future in water desalination, *Desalination*, 2014, **336**, 97–109.
11 H.-L. Li, Y.-X. Jia and Y.-D. Hu, Molecular dynamics simulation of the desalination of sea water by a forward osmosis membrane containing charged carbon nanotubes, *Acta Phys.-Chim. Sin.*, 2012, **28**(3), 573–577.
12 Y. Weizmann, D. M. Chenoweth and T. M. Swager, DNA– cnt nanowire networks for DNA detection, *J. Am. Chem. Soc.*, 2011, **133**(10), 3238–3241.
13 J. Wu, K. S. Paudek, C. Strasinger and B. J. Hinds, Programmable transdermal drug delivery of nicotine using carbon nanotube membranes, *Proc. Natl. Acad. Sci. U. S. A.*, 2010, **107**(26), 11698–11702.
14 N. E. Levinger, Water in confinement, *Science*, 2002, **298**(5599), 1722–1723.
15 N. Giovambattista, P. J. Rossky and P. G. Debenedetti, Phase transitions induced by nanoconfinement in liquid water, *Phys. Rev. Lett.*, 2009, **102**(5), 050603.
16 E. Tombari, G. Salvetti, C. Ferrari and G. P. Johari, Thermodynamic functions of water and ice confined to 2nm radius pores, *J. Chem. Phys.*, 2005, **122**, 104712.
17 A. Barati Farimani and N. R. Aluru, Existence of multiple phases of water at nanotube interfaces, *J. Phys. Chem. C*, 2016, **120**(41), 23763–23771.
18 A. Srivastava, S. Abedrabbo, J. Hassan and D. Homouz, Dynamics of confined water inside carbon nanotubes based on studying tetrahedral order parameters, *Sci. Rep.*, 2024, **14**(1), 15480.
19 M. Gordillo and J. Marti, Water on graphene surfaces, *J. Phys.: Condens. Matter*, 2010, **22**(28), 284111.
20 Y. Yun, R. Z. Khaliullin and Y. Jung, Low-dimensional confined ice has the electronic signature of liquid water, *J. Phys. Chem. Lett.*, 2019, **10**(8), 2008–2016.
21 G. Algara-Siller, O. Lehtinen, F. C. Wang, R. R. Nair, U. Kaiser, H. A. Wu, A. K. Geim and I. V. Grigorieva, Square ice in graphene nanocapillaries, *Nature*, 2015, **519**(7544), 443–445.
22 Z. He, J. Zhou, X. Lu and B. Corry, Ice-like water structure in carbon nanotube (8, 8) induces cationic hydration enhancement, *J. Phys. Chem. C*, 2013, **117**(21), 11412–11420.
23 F. Fang, S. Fu, J. Lin, J. Zhu, Z. Dai, G. Zhou and Z. Yang, Molecular-Level Insights into Unique Behavior of Water Molecules Confined in the Heterojunction between One-

and Two-Dimensional Nanochannels, *Langmuir*, 2022, **38**(23), 7300–7311.
24 J. Gillot, W. Bollmann and B. Lux, Cigar-shaped graphite crystals with conical structure, *Carbon*, 1968, **6**(3), 381.
25 W. Nazeer, A. Farooq, M. Younas, M. Munir and S. M. Kang, On molecular descriptors of carbon nanocones, *Biomolecules*, 2018, **8**(3), 92.
26 S. N. Naess, A. Elgsaeter and G. Helgesen, Carbon nanocones: wall structure and morphology, *Sci. Technol. Adv. Mater.*, 2009, **10**, 065002.
27 J.-C. Charlier and G.-M. Rignanese, Electronic structure of carbon nanocones, *Phys. Rev. Lett.*, 2001, **86**(26), 5970.
28 O. Shenderova, B. L. Lawson, D. Areshkin and D. W. Brenner, Predicted structure and electronic properties of individual carbon nanocones and nanostructures assembled from nanocones, *Nanotechnology*, 2001, **12**(3), 191.
29 J. Wei, K. M. Liew and X. He, Mechanical properties of carbon nanocones, *Appl. Phys. Lett.*, 2007, **91**, 26.
30 G. Paredes, C. Villeneuve-Faure and M. Monthioux, Carbon nanocone mechanical behavior and their use as AFM tips for the characterization of polymers in Peak Force mode, *Carbon*, 2024, **226**, 119076.
31 P.-C. Tsai and T.-H. Fang, A molecular dynamics study of the nucleation, thermal stability and nanomechanics of carbon nanocones, *Nanotechnology*, 2007, **18**(10), 105702.
32 W. Li, W. Wang, Y. Zhang, Y. Yan, P. Kral and J. Zhang, Highly efficient water desalination in carbon nanocones, *Carbon*, 2018, **129**, 374–379.
33 M. Razmkhah, A. Ahmadpour, M. T. Hamed Mosavian and F. Moosavi Baigi, What is the effect of carbon nanotube shape on desalination process? A simulation approach, *Desalination*, 2017, **407**, 103–115.
34 M. T. Baei, A. A. Peyghan and Z. Bagheri, Carbon nanocone as an ammonia sensor: DFT studies, *Struct. Chem.*, 2013, **24**, 1099–1103.
35 M. J. Sarvestani and R. Ahmadi, Adsorption of TNT on the surface of pristine and N-doped carbon nanocone: A theoretical study, *Asian J. Nanosci. Mater.*, 2020, **3**, 103–114.
36 N. Yang, G. Zhang and B. Li, Carbon nanocone: A promising thermal rectifier, *Appl. Phys. Lett.*, 2008, **93**(24), 243111.
37 K. Shoyama and F. Würthner, Synthesis of a carbon nanocone by cascade annulation, *J. Am. Chem. Soc.*, 2019, **141**(33), 13008–13012.
38 Q. Zhang, X. M. Xie, S. Y. Wei, Z. Z. Zhu, L. S. Zheng and S. Y. Xie, The synthesis of conical carbon, *Small Methods*, 2021, **5**(3), 2001086.
39 K. Skibińska and P. Żabiński, Nanocones: A Compressive Review of Their Electrochemical Synthesis and Applications, *Materials*, 2024, **17**(13), 3089.
40 G. Cicero, J. C. Grossman, E. Schwegler, F. Gygi and G. Galli, Water confined in nanotubes and between graphene sheets: A first principle study, *J. Am. Chem. Soc.*, 2008, **130**(6), 1871–1878.
41 M. Raju, A. Van Duin and M. Ihme, Phase transitions of ordered ice in graphene nanocapillaries and carbon nanotubes, *Sci. Rep.*, 2018, **8**(1), 3851.
42 N. Modeler, Generation of Nano-Geometries, *JCrystal Soft*, **http://www.jcrystal.com/products/wincnt**.
43 R. Dennington, T. Keith, and J. Millam, *GaussView*, version 5. 2009.
44 K. Momma and F. Izumi, VESTA 3 for three-dimensional visualization of crystal, volumetric and morphology data, *J. Appl. Crystallogr.*, 2011, **44**(6), 1272–1276.
45 W. L. Jorgensen, D. S. Maxwell and J. Tirado-Rives, Development and testing of the OPLS all-atom force field on conformational energetics and properties of organic liquids, *J. Am. Chem. Soc.*, 1996, **118**(45), 11225–11236.
46 H. J. Berendsen, J.-R. Grigera and T. P. Straatsma, The missing term in effective pair potentials, *J. Phys. Chem.*, 1987, **91**(24), 6269–6271.
47 H. W. Horn, W. C. Swope, J. W. Pitera, J. D. Madura, T. J. Dick, G. L. Hura and T. Head-Gordon, Development of an improved four-site water model for biomolecular simulations: TIP4P-Ew, *J. Chem. Phys.*, 2004, **120**(20), 9665–9678.
48 E. Jalalitalab, M. Abbaspour and H. Akbarzadeh, Thermodynamic, structural, and dynamical properties of nano-confined water using SPC/E and TIP4P models by molecular dynamics simulations, *New J. Chem.*, 2018, **42**(19), 16258–16272.
49 C. G. Ferrara and T. S. Grigera, Dynamics and structural behavior of water in large confinement with planar amorphous walls, *J. Chem. Phys.*, 2017, **147**, 024705.
50 J. Dix, L. Lue and P. Carbone, Why different water models predict different structures under 2D confinement, *J. Comput. Chem.*, 2018, **39**(25), 2051–2059.
51 S. Fei, W. L. Hsu, J. J. Delaunay and H. Daiguji, Molecular dynamics study of water confined in MIL-101 metal–organic frameworks, *J. Chem. Phys.*, 2021, **154**, 144503.
52 T. Nanok, N. Artrith, P. Pantu, P. A. Bopp and J. Limtrakul, Structure and dynamics of water confined in single-wall nanotubes, *J. Phys. Chem. A*, 2009, **113**(10), 2103–2108.
53 B. Hess, H. Bekker, H. J. C. Berendsen and J. G. E. M. Fraaije, LINCS: A linear constraint solver for molecular simulations, *J. Comput. Chem.*, 1997, **18**(12), 1463–1472.
54 C. Luo, X. Zuo, L. Wang, E. Wang, S. Song, J. Wang, J. Wang, C. Fan and Y. Cao, Flexible carbon nanotube– polymer composite films with high conductivity and superhydrophobicity made by solution process, *Nano Lett.*, 2008, **8**(12), 4454–4458.
55 G. Bussi, D. Donadio and M. Parrinello, Canonical sampling through velocity rescaling, *J. Chem. Phys.*, 2007, **126**(1), 014101.
56 H. J. C. Berendsen, J. P. M. Postma, W. F. van Gunsteren, A. DiNola, J. R. Haak, *et al.*, Molecular dynamics with coupling to an external bath, *J. Chem. Phys.*, 1984, **81**(8), 3684–3690.
57 A. K. Soper and M. G. Phillips, A new determination of the structure of water at 25°C, *Chem. Phys.*, 1986, **107**(1), 47–60.
58 A. Luzar and D. Chandler, Hydrogen-bond kinetics in liquid water, *Nature*, 1996, **379**(6560), 55–57.

59 A. Luzar and D. Chandler, Effect of Environment on Hydrogen Bond Dynamics in Liquid Water, *Phys. Rev. Lett.*, 1996, **76**(6), 928–931.
60 J. Teixeira and M. C. Bellissent-Funel, Dynamics of water studied by neutron scattering, *J. Phys.: Condens. Matter*, 1990, **2**, SA105–SA108.
61 I. Hanasaki and A. Nakatani, Hydrogen bond dynamics and microscopic structure of confined water inside carbon nanotubes, *J. Chem. Phys.*, 2006, **124**(17), 174714.
62 A. Debnath, B. Mukherjee, K. G. Ayappa, P. K. Maiti and S. T. Lin, Entropy and dynamics of water in hydration layers of a bilayer, *J. Chem. Phys.*, 2010, **133**, 174704.
63 M. G. Mazza, N. Giovambattista, F. W. Starr and H. E. Stanley, Relation between rotational and translational dynamic heterogeneities in water, *Phys. Rev. Lett.*, 2006, **96**(5), 057803.
64 T. A. Pascal, W. A. Goddard and Y. Jung, Entropy and the driving force for the filling of carbon nanotubes with water, *Proc. Natl. Acad. Sci. U. S. A.*, 2011, **108**(29), 11794–11798.
65 A. Srivastava, J. Hassan and D. Homouz, Hydrogen bond dynamics and phase transitions of water inside carbon nanotubes, *Nanomaterials*, 2023, **13**, 284.
66 T. Werder, J. H. Walther, R. L. Jaffe, T. Halicioglu, F. Noca and P. Koumoutsakos, Molecular dynamics simulation of contact angles of water droplets in carbon nanotubes, *Nano Lett.*, 2001, **1**(12), 697–702.
67 S. Han, M. Y. Choi, P. Kumar and H. E. Stanley, Phase transitions in confined water nanofilms, *Nat. Phys.*, 2010, **6**(9), 685–689.
68 T. Kaneko, J. Bai, K. Yasuoka, A. Mitsutake and C. X. Zeng, Liquid-solid and solid-solid phase transition of monolayer water: High-density rhombic monolayer ice, *J. Chem. Phys.*, 2014, **140**(18), 184507.
69 W. Du, Y. Wang, J. Yang and J. Chen, Two rhombic ice phases from aqueous salt solutions under graphene confinement, *Phys. Rev. E*, 2024, **109**(6), L062103.
70 D. Shin, J. Hwang and W. Jhe, Ice-VII-like molecular structure of ambient water nanomeniscus, *Nat. Commun.*, 2019, **10**(1), 286.
71 D. Shin, H. Seo and W. Jhe, Exploring the Hydration Water Character on Atomically Dislocated Surfaces by Surface Enhanced Raman Spectroscopy, *ACS Cent. Sci.*, 2020, **6**(11), 2079–2087.
72 T. R. Jensen, M. Østergaard Jensen, N. Reitzel, K. Balashev, G. H. Peters, K. Kjaer and T. Bjørnholm, Water in contact with extended hydrophobic surfaces: direct evidence of weak dewetting, *Phys. Rev. Lett.*, 2003, **90**(8), 086101.
73 T. Kim, G. W. Kim, H. Jeong, G. Kim and S. Jang, Equilibrium structures of water molecules confined within a multiply connected carbon nanotube: a molecular dynamics study, *Phys. Chem. Chem. Phys.*, 2020, **22**(1), 252–257.
74 S. Dalla Bernardina, E. Paineau, J. B. Brubach, P. Judeinstein, S. Rouzière, P. Launois and P. Roy, Water in carbon nanotubes: the peculiar hydrogen bond network revealed by infrared spectroscopy, *J. Am. Chem. Soc.*, 2016, **138**(33), 10437–10443.
75 S. Strazdaite, J. Versluis and H. J. Bakker, Water orientation at hydrophobic interfaces, *J. Chem. Phys.*, 2015, **143**(8), 084708.
76 M. F. Harrach and B. Drossel, Structure and dynamics of TIP3P, TIP4P, and TIP5P water near smooth and atomistic walls of different hydroaffinity, *J. Chem. Phys.*, 2014, **140**(17), 174501.
77 K. G. Ayappa, Enhancing the Dynamics of Water Confined between Graphene Oxide Surfaces with Janus Interfaces: A Molecular Dynamics Study, *J. Phys. Chem. B*, 2019, **123**(13), 2978–2993.
78 A. T. Sose, E. Mohammadi, F. Wang and S. A. Deshmukh, Investigation of structure and dynamics of water confined between hybrid layered materials of graphene, boron nitride, and molybdenum disulfide, *J. Mater. Sci.*, 2022, **57**(23), 10517–10534.
79 G. Karataraki, A. Sapalidis, E. Tocci and A. Gotzias, Molecular Dynamics of Water Embedded Carbon Nanocones: Surface Waves Observation, *Computation*, 2019, **7**(3), 50.
80 Q. Wang, L. Liu, C. Liu, J. Song and X. Gao, Size effect in determining the water diffusion rate in carbon nanotubes, *J. Mol. Liq.*, 2021, **334**, 116034.
81 M. Nazari, A. Davoodabadi, D. Huang, T. Luo and H. Ghasemi, Transport Phenomena in Nano/Molecular Confinements, *ACS Nano*, 2020, **14**(12), 16348–16391.
82 A. Zaragoza, M. A. González, L. Joly, I. López-Montero, M. A. Canales, A. L. Benavides and C. Valeriani, Molecular dynamics study of nanoconfined TIP4P/2005 water: how confinement and temperature affect diffusion and viscosity, *Phys. Chem. Chem. Phys.*, 2019, **21**(25), 13653–13667.
83 R. Horstmann, L. Hecht, S. Kloth and M. Vogel, Structural and Dynamical Properties of Liquids in Confinements: A Review of Molecular Dynamics Simulation Studies, *Langmuir*, 2022, **38**(21), 6506–6522.
84 Y. Qiu, L. Lupi and V. Molinero, Is water at the graphite interface vapor-like or ice-like?, *J. Phys. Chem. B*, 2018, **122**(13), 3626–3634.
85 K. Laasonen, M. Sprik, M. Parrinello and R. Car, "Ab initio'' liquid water, *J. Chem. Phys.*, 1993, **99**(11), 9080–9089.
86 W. Zhao, H. Qiu and W. Guo, A Deep Neural Network Potential for Water Confined in Graphene Nanocapillaries, *J. Phys. Chem. C*, 2022, **126**(25), 10546–10553.
87 S. P. Kadaoluwa Pathirannahalage, N. Meftahi, A. Elbourne, A. C. G. Weiss, C. F. McConville, A. Padua, D. A. Winkler, M. C. Gomes, T. L. Greaves, T. C. Le, Q. A. Besford and A. J. Christofferson, Systematic Comparison of the Structural and Dynamic Properties of Commonly Used Water Models for Molecular Dynamics Simulations, *J. Chem. Inf. Model.*, 2021, **61**(9), 4521–4536.
88 Y. Zhang, J. Tian, H. Huang, C. Sun, C. Li, G. Li, D. Ji, Z. Fan and L. Pan, New insights into the role of nitrogen doping in microporous carbon on the capacitive charge storage

mechanism: From ab initio to machine learning accelerated molecular dynamics, *Carbon*, 2024, **229**, 119498.

89 R. Hou, C. Li and D. Pan, Raman and IR spectra of water under graphene nanoconfinement at ambient and extreme pressure–temperature conditions: a first-principles study, *Faraday Discuss.*, 2024, **249**, 181–194.

90 J. Zubeltzu and E. Artacho, Simulations of water nanoconfined between corrugated planes, *J. Chem. Phys.*, 2017, **147**(19), 194509.

91 D. Muñoz-Santiburcio and D. Marx, Nanoconfinement in Slit Pores Enhances Water Self-Dissociation, *Phys. Rev. Lett.*, 2017, **119**(5), 056002.

92 D. Muñoz-Santiburcio and D. Marx, Chemistry in nanoconfined water, *Chem. Sci.*, 2017, **8**(5), 3444–3452.